PHYSICAL REVIEW D **85,** 127502 (2012)

Erratum and Addendum: Gravitational waves from black hole-neutron star binaries: Classification of waveforms

Masaru Shibata,[1] Koutarou Kyutoku,[2] Tetsuro Yamamoto,[3] and Keisuke Taniguchi[4]

[1]*Yukawa Institute of Theoretical Physics, Kyoto University, Kyoto 606-8502, Japan*
[2]*Theory Center, Institute of Particles and Nuclear Studies, KEK, Tsukuba, Ibaraki 305-0801, Japan*
[3]*Yugen Club, Toyama, Shinjuku, Tokyo 162-0052, Japan*
[4]*Graduate School of Arts and Sciences, The University of Tokyo, Tokyo 153-8902, Japan*
(Received 18 November 2011; published 19 June 2012)

A coding error was found in our original version of numerical-relativity code SACRA. We correct the results of [M. Shibata, K. Kyutoku, T. Yamamoto, and K. Taniguchi, Phys. Rev. D **79**, 044030 (2009).] by simulations of the improved accuracy.

DOI: 10.1103/PhysRevD.85.127502 PACS numbers: 04.25.D−, 04.30.−w, 04.40.Dg, 99.10.Cd

In [1], we reported numerical results obtained by our SACRA code employing a simple Γ-law equation of state with $\Gamma = 2$. During subsequent studies [2,3], we noticed that we systematically *underestimated* disk masses in the original work. The reason is that we evolved hydrodynamic variables and estimated disk masses only in a domain of the size $\sim 200^3$ km^3, although Einstein's equations were solved in domains of size $\sim 1500^3$–2000^3 km^3. A small-size domain for hydrodynamics is insufficient for the estimation of the disk mass, if tidal disruption occurs. In particular, for a large neutron star (NS) radius, the tidally disrupted material extends far away from the central region, and the disk mass was significantly underestimated. This problem was found during the writing of [3], and the erratum of [2,4] were already published.

For this reason, we reperformed simulations for the same models as those of [1], enlarging the computational domain of hydrodynamics. To estimate disk masses more accurately, in addition, we improved the grid resolutions from $N \leq 36$ (we use the same notations as used in [1]) to $N = 40$, 50, and 60; with $N = 60$, the diameters of NSs are covered by ≈ 100 grid points, and the diameters of apparent horizons of black holes (BHs) are by $\approx 20Q$ grid points. With this improved grid resolution, we also reanalyzed gravitational waves. In addition, the fitting formula for the quasinormal-mode frequency is updated to the latest, more sophisticated one derived in [5].

First, we show the convergence properties of our updated simulations. Figure 1 plots the merger time for $Q = 2$ models as a function of $1/N^2 (\propto \Delta x^2)$, and indicates that it converges approximately at the second order, which is expected for SACRA. Thus, a reasonable convergence is indicated to be achieved in our new simulations. The convergence properties of other quantities are discussed below.

The corrected quantities for the merger remnant are listed in Table I for three grid resolutions. This shows that an approximate convergence of the disk mass is achieved for cases $M_{r>r_{\rm AH}} \gtrsim 0.01M_*$, and the convergence appears to be not so good when $M_{r>r_{\rm AH}} \lesssim 0.01M_*$. This is simply because such a small disk mass is supplied from a lower-density region near the surface of NSs for which an accurate computation is forbidden in a poor-resolution run; i.e., the steep density gradients near the surface cannot be accurately resolved, leading to a slight spurious expansion of the surface which spuriously increases the resulting disk mass. We estimate that the disk mass is overestimated even in the run with $N = 60$ by a factor of 2–3, when the resulting disk mass is of order $10^{-3}M_*$ or less. Figure 2 plots the evolution of $M_{r>r_{\rm AH}}$ for three grid resolutions. This indeed indicates that the convergence is good when $M_{r>r_{\rm AH}} \gtrsim 0.01M_*$ but not as good when $M_{r>r_{\rm AH}} \sim 10^{-3}M_*$. Although the remnant disk mass may be overestimated by $10^{-3}M_*$–$10^{-2}M_*$, this error is acceptable for the problem of disk formation with $\sim 0.1M_*$. We also note that our results of the disk mass for models M30.145 are in approximate agreement with those of numerical-relativity simulations performed by other two groups [6,7].

Table I shows that corrected quantities of the remnant BH are in the convergent regime within $O(0.1)\%$ errors except for a_{f1}, indicating a reasonable convergence.

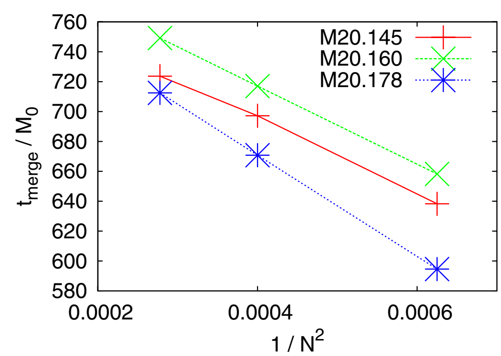

FIG. 1 (color online). The merger time normalized by the Arnowitt-Deser-Misner mass of the initial configuration for models with $Q = 2$ as a function of $1/N^2$. The left, middle, and right points correspond to the results of $N = 60$, 50, and 40, respectively.

TABLE I. Corrected numerical results for the remnants: Compare with Table III of [1].

Model	$M_{r>r_{\rm AH}}/M_*$	$M_{\rm BH,f}/M_0$	$C_e/4\pi M_0$	$M_{\rm irr}/M_0$	C_p/C_e	$a_{\rm f1}$	$a_{\rm f2}$	$a_{\rm f3}$	$f_{\rm cut}m_0$
M20.145 ($N=60$)	0.060	0.970	0.970	0.903	0.898	0.692	0.682	0.683	0.036
M20.145 ($N=50$)	0.065	0.969	0.968	0.902	0.899	0.693	0.679	0.680	0.037
M20.145 ($N=40$)	0.066	0.969	0.969	0.901	0.898	0.703	0.682	0.680	0.034
M20.160 ($N=60$)	0.021	0.981	0.980	0.912	0.897	0.694	0.684	0.685	0.055
M20.160 ($N=50$)	0.025	0.980	0.980	0.911	0.897	0.697	0.684	0.685	0.054
M20.160 ($N=40$)	0.028	0.980	0.979	0.910	0.897	0.704	0.684	0.685	0.052
M20.178 ($N=60$)	0.0021	0.983	0.982	0.917	0.903	0.680	0.667	0.667	0.078
M20.178 ($N=50$)	0.0027	0.984	0.982	0.917	0.905	0.688	0.666	0.662	0.075
M20.178 ($N=40$)	0.0067	0.984	0.982	0.916	0.902	0.701	0.670	0.662	0.069
M30.145 ($N=60$)	0.044	0.978	0.978	0.936	0.936	0.566	0.556	0.557	0.065
M30.145 ($N=50$)	0.047	0.978	0.978	0.935	0.936	0.585	0.557	0.558	0.063
M30.145 ($N=40$)	0.055	0.977	0.976	0.934	0.936	0.573	0.556	0.558	0.056
M30.160 ($N=60$)	0.014	0.982	0.982	0.940	0.937	0.565	0.554	0.555	0.080
M30.160 ($N=50$)	0.017	0.982	0.981	0.939	0.937	0.569	0.554	0.555	0.079
M30.160 ($N=40$)	0.023	0.982	0.981	0.939	0.936	0.578	0.556	0.555	0.075
M30.178 ($N=60$)	0.0011	0.983	0.982	0.941	0.938	0.561	0.547	0.548	0.086
M30.178 ($N=50$)	0.0020	0.983	0.982	0.941	0.938	0.568	0.549	0.550	0.086
M30.178 ($N=40$)	0.0039	0.984	0.983	0.941	0.937	0.580	0.551	0.550	0.083
M40.145 ($N=60$)	0.016	0.986	0.985	0.955	0.955	0.485	0.475	0.477	0.080
M40.145 ($N=50$)	0.018	0.985	0.985	0.955	0.955	0.486	0.475	0.476	0.079
M40.145 ($N=40$)	0.026	0.985	0.984	0.954	0.955	0.492	0.474	0.476	0.076
M50.145 ($N=60$)	4×10^{-4}	0.990	0.989	0.966	0.966	0.426	0.417	0.418	0.082
M50.145 ($N=50$)	7×10^{-4}	0.990	0.989	0.967	0.965	0.431	0.418	0.420	0.082
M50.145 ($N=40$)	0.0022	0.991	0.990	0.966	0.965	0.435	0.419	0.420	0.080

The reason for the poorer convergence of $a_{\rm f1}$ is due to its dependence on the mass and angular momentum of the remnant disk. However, we find that the disagreement between $a_{\rm f1}$ and other two, $a_{\rm f2}$ and $a_{\rm f3}$, becomes smaller as the grid resolution is improved, and the error is $\lesssim 0.015$ for $N=60$. We note that $M_{\rm BH,f}$ and $C_e/4\pi$ always agree approximately with each other irrespective of N.

The corrected remnant disk mass for $N=60$ is significantly larger than that in our previous simulations. The reason for the mistake in [1] is due to the fact that we did not follow the motion of the material which is ejected by tidal disruption and escapes outside the central domain of the size $\sim 200^3$ km^3, even when they are bound and supposed to eventually return to the neighborhood of the BH. The new SACRA can correctly estimate the mass of the returned material. Snapshots of the rest-mass density profiles for model M30.145 are displayed in Fig. 3, which shows that the hydrodynamics processes are solved appropriately in the far region. Figure 4 plots the time evolution of $M_{r>r_{\rm AH}}$ for all the models with $N=60$. It is found that the remnant disk mass after ≈ 10 ms of the merger exceeds $0.01M_\odot$ for a wider range of binary parameters (for a hypothetical NS mass $1.35M_\odot$). However, the remnant disk mass is still small for a large mass ratio, $Q=5$ or for a compact NS, $\mathcal{C}=0.178$ for which the tidal effect plays a minor role in the merger process.

By contrast, quantities associated with the remnant BH do not differ much from those obtained in [1]. This fact suggests that the disrupted material does not affect the remnant BH strongly. This is reasonable, because the mass of the remnant BH is always much larger than that of the remnant disk.

The gravitational waveforms for selected models are plotted in Fig. 5. As often found in our series of papers [2,3], the waveform agrees well with the Taylor-T4 formula

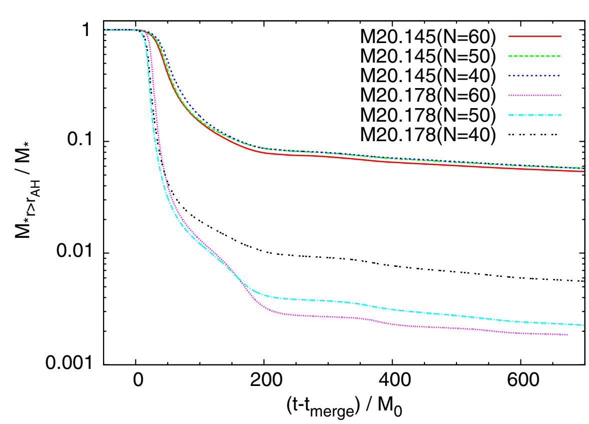

FIG. 2 (color online). Evolution of the rest mass of the material located outside the apparent horizon for different grid resolutions of models M20.145 and M20.178.

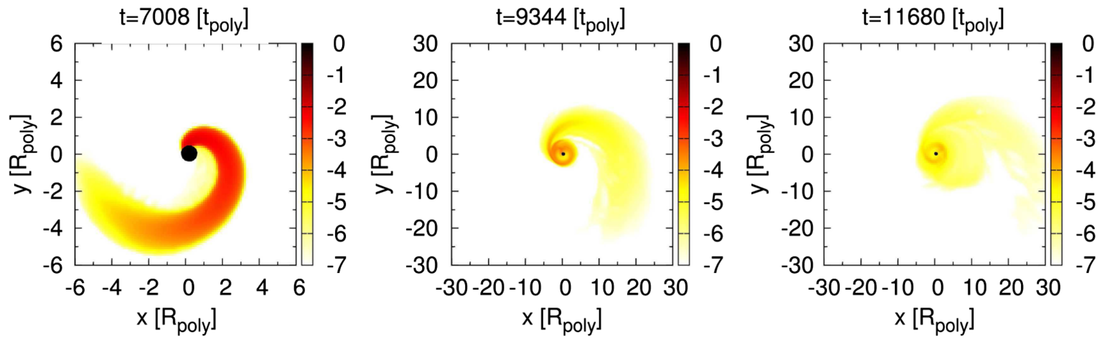

FIG. 3 (color online). Evolution of the rest-mass density profile in the logarithmic scale and the location of apparent horizons (black filled circles) for model M30.145 ($N = 60$). All the quantities are shown in the polytropic unit, in which the unit length is $\approx$ 14 km for a hypothetical NS mass $M_{\rm NS} = 1.35 M_\odot$.

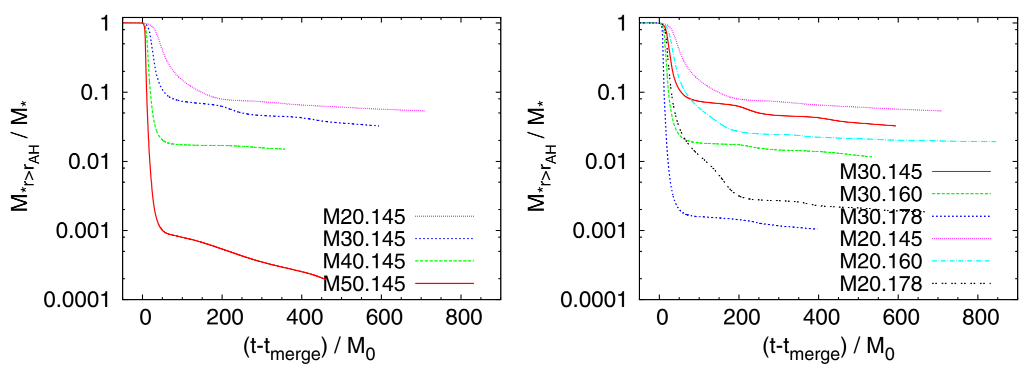

FIG. 4 (color online). Left: Evolution of the rest mass of the material located outside apparent horizons for models M20.145, M30.145, M40.145, and M50.145 in $N = 60$ runs. Right: The same as the left panel, but for models M30.145, M30.160, M30.178, M20.145, M20.160, M20.178 in $N = 60$ runs. For a hypothetical NS mass $M_{\rm NS} = 1.35 M_\odot$, $100 M_0 \approx 2.00(Q + 1)/3$ ms.

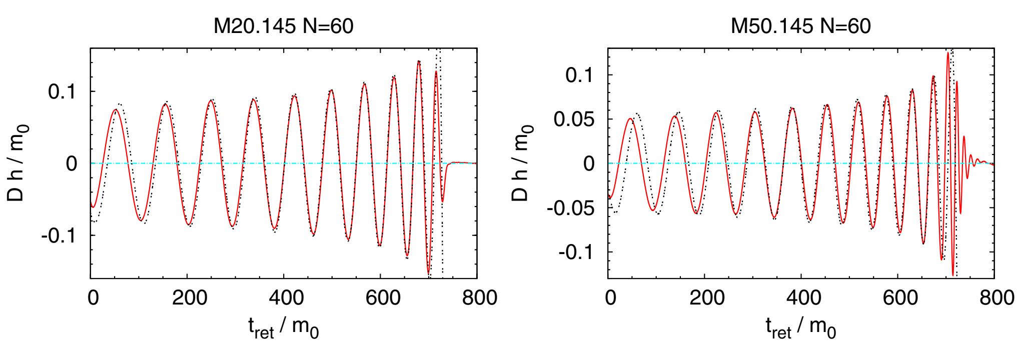

FIG. 5 (color online). Gravitational waveforms observed along the z axis (solid curve) for models M20.145 (left) and M50.145 (right). $t_{\rm ret}$ denotes the retarded time and m_0 is the total mass. The solid curves denote the results obtained in $N = 60$ runs and the dot-dotted curves denote the waveforms derived by the Taylor-T4 formula.

except for the first one orbit and for the final inspiral orbit just before the merger. For completeness, corrected results for the radiated energy and angular momentum are also listed in Table II.

The gravitational-wave spectra for selected models are shown in the left panel of Fig. 6 together with the spectra computed by the Taylor-T4 formula and of the phenomenological waveform proposed in [8] following the idea

TABLE II. Corrected numerical results for gravitational waves: Compare with Table IV of [1].

Model	$\Delta E/M_0$(%)	$\Delta J/J_0$(%)	(2,2)	(3,3)	(4,4)	(2,1)	$f_{\rm QNM}M_{\rm BH}$	$V_{\rm kick}$ (km/s)
M20.145 ($N = 60$)	0.80	17	0.78	0.014	0.004	0.001	0.084	25
M20.160 ($N = 60$)	1.13	20	1.10	0.024	0.007	0.003	0.084	43
M20.178 ($N = 60$)	1.62	23	1.56	0.037	0.010	0.008	0.083	80
M30.145 ($N = 60$)	0.99	18	0.93	0.041	0.009	0.003	0.077	20
M30.160 ($N = 60$)	1.37	22	1.28	0.068	0.012	0.007	0.077	15
M30.178 ($N = 60$)	1.70	24	1.56	0.11	0.017	0.010	0.077	40
M40.145 ($N = 60$)	1.09	20	0.97	0.084	0.018	0.016	0.073	92
M50.145 ($N = 60$)	1.01	20	0.86	0.11	0.022	0.012	0.071	84

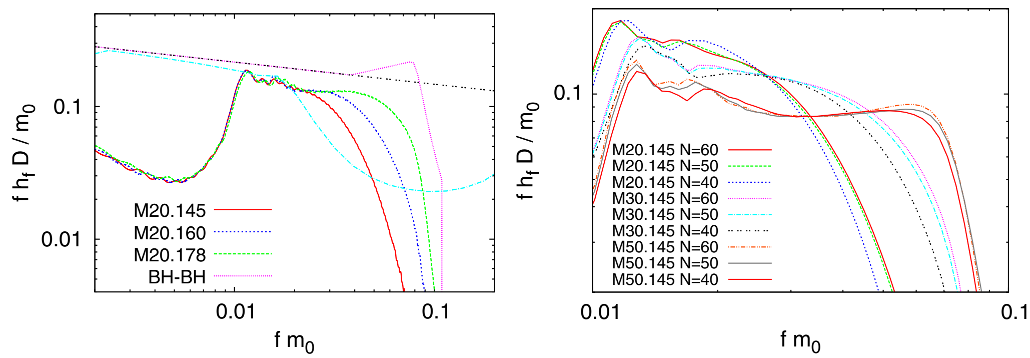

FIG. 6 (color online). Left: The spectrum of gravitational waves $fh(f)D/m_0$ for models M20.145, M20.160, and M20.178 with $N = 60$. The dashed and long-dashed curves denote spectra computed in the quadrupole and Taylor-T4 formulae, respectively. The curve labeled "BH-BH" is the spectrum of the phenomenological waveform for binary black holes proposed in [8]. Right: The spectra for models M20.145, M30.145, and M50.145 with different grid resolutions. We do not match numerical data to the Taylor-T4 waveform unlike in our original paper.

of [7]. We also recomputed the cutoff frequency, $f_{\rm cut}$, for each model, and the results are listed in Table. I. We reconfirm the correlation between $\mathcal{C}$ and $f_{\rm cut}m_0$ for the fixed Q (the cutoff frequency converges approximately for $N = 60$ and 50). The right panel of Fig. 6 shows the spectrum for selected models with different grid resolutions, and indicates that the spectrum is in the convergent regime for $N = 60$ and 50.

Finally, we would like to apologize to readers of [1] for any inconvenience caused by our negligence.

[1] M. Shibata, K. Kyutoku, T. Yamamoto, and K. Taniguchi, Phys. Rev. D **79**, 044030 (2009).

[2] K. Kyutoku, M. Shibata, and K. Taniguchi, Phys. Rev. D **82**, 044049 (2010).

[3] K. Kyutoku, H. Okawa, M. Shibata, and K. Taniguchi, Phys. Rev. D **84**, 064018 (2011).

[4] K. Kyutoku, M. Shibata, and K. Taniguchi, Phys. Rev. D **84**, 049902(E) (2011).

[5] E. Berti, V. Cardoso, and A. O. Starinets, Classical Quantum Gravity **26**, 163001 (2009).

[6] M. D. Duez, F. Foucart, L. E. Kidder, C. D. Ott, and S. A. Teukolsky, Classical Quantum Gravity **27**, 114106 (2010).

[7] Z. B. Etienne, Y. T. Liu, S. L. Shapiro, and T. W. Baumgarte, Phys. Rev. D **79**, 044024 (2009).

[8] P. Ajith, S. Babak, Y. Chen, M. Hewitson, B. Krishnan, A. M. Sintes, J. T. Whelan, B. Brügmann, P. Diener, N. Dorband *et al.*Phys. Rev. D **77**, 104017 (2008).